

Effective potential and topological photon spheres: a novel approach to black hole parameter classification

Mohammad Ali S. Afshar^{1,2†}  Jafar Sadeghi^{1,2‡}

¹Department of Physics, Faculty of Basic Sciences, University of Mazandaran 47416-95447, Babolsar, Iran

²Canadian Quantum Research Center, 204-3002 32 Ave Vernon, BC V1T 2L7, Canada

Abstract: In this paper, we base our analysis on the assumption that the existence of a photon sphere is an intrinsic characteristic of any ultra-compact gravitational structure with spherical symmetry. Utilizing the concept of a topological photon sphere, we categorize the behaviors of various gravitational models based on the structure of their photon spheres. This innovative approach enables us to define boundaries for black hole parameters, subsequently enabling us to classify the model as either a black hole or naked singularity. We demonstrate that the presence of this interplay between the gravitational structure and the existence of a photon sphere is a unique advantage that can be utilized from both perspectives. Our observations indicate that a gravitational model typically exhibits the behavior of a horizonless structure (or naked singularity) when a minimum effective potential (a stable photon sphere) appears within the studied spacetime region. Additionally, in this study, we investigate the effect of this structure on the behavior of the photon sphere by selecting models that are affected by Perfect Fluid Dark Matter (PFDM). Finally, by analyzing a model with multiple event horizons, we show that the proposed method remains applicable even in such scenarios.

Keywords: black hole, photon sphere, topological classification, different parameters

DOI: 10.1088/1674-1137/ada127 **CSTR:** 32044.14.ChinesePhysicsC.49035107

I. INTRODUCTION

In the study of ultra-compact gravitational objects, the simplest and most fundamental step to distinguish between different configurations is to examine the metric function and subsequently identify the event horizon. The metric function is essentially the result of integrating equations based on diverse and complex initial conditions (such as energy conditions and geometric compatibility with general relativity equations). Any remaining weaknesses that might challenge the physics of the derived model are addressed by conjectures such as the Weak Cosmic Censorship Conjecture (WCCC), which posits the creation of an event horizon. This conjecture assumes that singularities emerging from solving Einstein's equations must be hidden behind an event horizon. This is because if singularities were observable from the rest of spacetime, causality would be compromised, and physics would lose its predictive power. Note that the failure to satisfy the WCCC condition does not imply "non-existence" or "absence," but rather the "existence" of a spacetime that, although it has its own gravitational effects, our current knowledge is insufficient to decode. Ex-

tensive studies are currently being conducted on the possibility and conditions for the emergence and observation of these regions. For instance, spacetime singularities formed during gravitational collapse can be observed by an external observer, and the observability of a spacetime singularity depends on the initial conditions of the collapsing matter [1–14]. Therefore, the conditions under which our model behaves like a black hole and from what range it transitions to an ultra-compact object without an event horizon (naked singularity) must be known. However, naked singularity regions may also be involved under certain conditions in the results. Hence, their extent of influence must also be determined.

After the initial metric function is constructed, the most significant factor influencing the location of the event horizon is the values assigned to the parameters of each theory used in constructing the metric function. In a simplified view, the permissible range of these parameters can be studied based on the roots of the metric function. Because all necessary conditions, including the geometric equations of general relativity and energy conditions, have been integrated within the system of equations, the result has manifested as a model characterized

Received 2 December 2024; Accepted 19 December 2024; Published online 20 December 2024

[†] E-mail: m.a.s.afshar@gmail.com

[‡] E-mail: pouriya@ipm.ir

©2025 Chinese Physical Society and the Institute of High Energy Physics of the Chinese Academy of Sciences and the Institute of Modern Physics of the Chinese Academy of Sciences and IOP Publishing Ltd. All rights, including for text and data mining, AI training, and similar technologies, are reserved.

by a defined metric function. However, this method cannot be used to determine the dominance range of a naked singularity. Therefore, to gain a better understanding of the overall space surrounding an ultra-compact object, we must seek a potential function that provides a more comprehensive response to the effect of the gravity of this structure on the entire surrounding space. In pursuit of such a function, we know that the nature of gravitational structures, whether in their classical or quantum forms, necessitates the existence of stable and unstable circular orbits. Moreover, in gravity, the existence of such orbits around a black hole or an ultra-compact object has been extensively calculated both experimentally and observationally, as well as theoretically for various black hole models. For example, in an observational study, investigators documented the presence of a distinct dark shadow, which emerged owing to the gravitational deflection of light by the colossal black hole located at the nucleus of the massive elliptical galaxy M87. This phenomenon conclusively substantiates the existence of photon rings encircling the central dense object [15–20]. Additionally, Cunha et al. theoretically showed that, in spherical symmetry, standard black holes, as well as other ultra-compact objects (that can be with or without event horizon) in general relativity, can have planar circular photon orbits such that the stable type causes instability, and its unstable type can determine the shadows of the black hole [21]. Moreover, a new paper has shown in a geometrical proof that "any spherically symmetric space-time that is asymptotically flat and has a horizon must contain a photon sphere, a spherical photon shell" [22]. Therefore, considering the above characteristics, the concept of the photon sphere may be used for a more precise classification of the space surrounding the ultra-compact structures.

As stated earlier, the foundation of our work in this article is predicated on the necessity of the photon sphere for ultra-compact object structures. However, to approach the topological photon sphere historically, we commence our study of the photon sphere from the point at which Cardoso et al. have articulated, "The mere observation of an unstable light ring is strong evidence for the existence of black holes," or, "The existence of a stable light ring is thus an unavoidable feature of any ultra-compact star" [23]. Subsequently, Cunha et al. showed that, in spherical symmetry, standard black holes, as well as other ultra-compact objects (that can be with or without event horizon) in general relativity, can have planar circular photon orbits such that the stable type causes instability, and its unstable type can determine the shadows of the black hole [22]. Finally, after Cunha et al. extended their work to spherically symmetric 4D black holes [24], Wei used this concept and Duan mapping to extend the discussion of the photon ring to the photon sphere with a topological approach. He stated that at least one standard

photon sphere exists outside the black hole, not only in asymptotically flat space-time but also in asymptotically Anti-de Sitter (AdS) and de Sitter (dS) space-time [25].

In this article, we use the "Wei method" to classify space based on the topological photon sphere behavior for different black holes. This means that the topological current is non-zero only at the zero point of the vector field, which determines the location of the photon sphere. Therefore, one topological charge can be considered for each photon sphere. In the full exterior region, based on a specific range of parameters in which the Total Topological Charge (TTC) is always equal to -1 , the structure will be considered a black hole, and conversely. Moreover, on the same basis, for a naked singularity that has a vanishing topological charge, the TTC will be 0 [25] or $+1$ [26]. Ultimately, if neither of the above states occurs, these areas will likely represent forbidden zones. Forbidden in the sense that both the metric function has no roots and the potential function exhibits no gravitational effect on photons. An essential point to emphasize before the end of this section is that in this article, we utilize the effective potential whose notable characteristic is that it solely depends on the geometry and structure of spacetime without relying on the properties of the incoming particle. We examine the existence of photon spheres in two scenarios: structures with an event horizon (black holes) and those without an event horizon (naked singularities). In addition to identifying the locations of these spheres and demonstrating the behavioral alignment of topological charge with the geometric behavior of the potential function, we show how the permissible range for each parameter must be defined for the structure to mathematically manifest as either a black hole or naked singularity. Note that our discussion is fundamentally based on the gravitational influence of the model on the motion of photons and massless particles, as well as the structure of null geodesics. Although the existence of these orbits is a necessary condition for the structure of an ultra-gravitational object, this does not imply that the obtained range necessarily holds a completely physical meaning. This range will be most meaningful when interpreted alongside other physical conditions and constraints. Overall, this method can provide a comprehensive view of the behavior of ultra-gravitational structures and serve as an auxiliary equation, thus offering better insights into the impact of the effective components in the black hole dynamics of the model.

The remainder of the paper is organized as follows. In Section II, we briefly review the mathematical and physical foundations of the work. Duan's topological mapping and the effective potential are introduced, and then the circular null geodesic conditions are presented. Finally, we combine the obtained relations and deduce the used calculation. In Section III, we first address the advantages and disadvantages of utilizing this method and

study the effective potential with greater precision in terms of physical concepts and the alignment of its graphical results with the TTC outcomes. We endeavor to articulate the physical significance of the effective potential graph. In Section IV, we study and analyze different introduced models using this method. Finally, the conclusions are given in Section V.

II. TOPOLOGICAL PATH TO THE PHOTON SPHERE

Solving the metric function (1) based on the specific parameters leads to only an interval in which the radius of event horizon will remain real according to the desired parameters,

$$ds^2 = -dt^2 f(r) + \frac{dr^2}{g(r)} + (d\theta^2 + d\varphi^2 \sin^2(\theta)) h(r). \quad (1)$$

The event horizon, a null one-sided hypersurface, acts as a causal boundary, ensuring that the WCCC holds. However, other areas exist in which system behavior is still important to us (for example, naked singularities, which are hypothetical gravitational singularities without an event horizon). The above statements indicate that there exists regions in which the behavior of the system is singular, and the metric function cannot aid us in identifying these regions. Therefore, we must utilize concepts that exhibit the gravitational behavior of the model under study with greater precision and over a broader area. Consequently, we explore the photon ring and photon sphere. The photon sphere is a null ring that is the lower bound for any stable orbit, exhibiting extreme bending of light rays in a very strong gravity. Two types exist: unstable, where small perturbations cause the photons to either escape or fall into the black hole, and stable, where the opposite occurs. The unstable type is useful for determining black hole shadows, whereas the stable type causes spacetime instability [27].

Several methods can be used to study the photon sphere. In this paper, we consider Wei's topological method [25]. To analyze the foundations of the work of this, we combine basic concepts such as Poincaré section [28], Duan's topological current mapping theory, and the necessary conditions for the existence of null geodesics.

In 1984, Duan conducted a pivotal analysis of the intrinsic structure of conserved topological currents within the $SU(2)$ gauge theory. During this examination, Duan introduced the concept of topological flow associated with point-like systems akin to particles. This foundational study laid the basis for subsequent discussions on various forms of topological currents [29]. In the first step, we consider a general vector field as ϕ , which can be decomposed into two components, ϕ^r and ϕ^θ :

$$\phi = (\phi^r, \phi^\theta), \quad (2)$$

Additionally, we can rewrite the vector as $\phi = \|\phi\|e^{i\theta}$, where $\|\phi\| = \sqrt{\phi^a \phi^a}$, or $\phi = \phi^r + i\phi^\theta$. Based on this, the normalized vector is defined as

$$n^a = \frac{\phi^a}{\|\phi\|}, \quad (3)$$

where $a = 1, 2$ and $(\phi^1 = \phi^r)$, $(\phi^2 = \phi^\theta)$. Now, we introduce our antisymmetric superpotential as follows [25, 29]:

$$\Upsilon^{\mu\nu} = \frac{1}{2\pi} \epsilon^{\mu\nu\rho} \epsilon_{ab} n^a \partial_\rho n^b, \quad \mu, \nu, \rho = 0, 1, 2$$

and the topological current becomes

$$j^\mu = \partial_\nu \Upsilon^{\mu\nu} = \frac{1}{2\pi} \epsilon^{\mu\nu\rho} \epsilon_{ab} \partial_\nu n^a \partial_\rho n^b.$$

Based on this, Noether's current and charges at the given Ω will be

$$\partial_\nu j^\nu = 0$$

and

$$Q = \int_\Omega j^0 d^2x, \quad (4)$$

where j^0 is the charge density. By replacing ϕ instead of n and using the Jacobi tensor, we obtain

$$j^\mu = \frac{J^\mu(X) \ln(\|\phi\|) \Delta_{\phi^a}}{2\pi}, \quad (5)$$

where $X = \frac{\phi}{x}$. By using two-dimensional Laplacian Green function in ϕ -mapping space, we have

$$\ln(\|\phi\|) \Delta_{\phi^a} = 2\delta(\phi)\pi, \quad (6)$$

and the topological current is

$$j^\mu = J^\mu(X) \delta^2(\phi). \quad (7)$$

The properties of δ show that j^μ is non-zero only at the zero points of ϕ^a , and this is exactly what we require to continue the discussion. Finally, by using the above relations and inserting them in relation (3), the topological charge becomes

$$Q = \int_{\Omega} J^0(X) \delta^2(\phi) d^2x, \quad (8)$$

Again and owing to the topological charge Q , according to the characteristic of the δ function, the charge can be considered to be non-zero only at the zero point of ϕ . This results will enable us to use and calculate the photon sphere in the near future.

Now, we will investigate the photon sphere and some null geodesics with a static and spherical symmetry background (1). The Lagrangian assumes the form [23]

$$\mathcal{L} = \dot{x}^\nu \dot{x}^\mu g_{\mu\nu} = \dot{t}^2 f(r) - \frac{\dot{r}^2}{g(r)} - \dot{\phi}^2 h(r),$$

where the dot denotes a derivative with respect to an affine parameter. Now, deriving the four-momentum from this Lagrangian, we have

$$p_\mu = \frac{\partial}{\partial \dot{x}^\mu} \mathcal{L} = \dot{x}^\nu g_{\mu\nu},$$

or more precisely

$$\begin{aligned} p_t &= \dot{t} f(r) \equiv E, \\ p_\phi &= -\dot{\phi} h(r) \equiv -L, \\ p_r &= -\frac{\dot{r}}{g(r)}. \end{aligned}$$

Here, E and L are the energy and angular momentum, respectively. As evident from the Lagrange equation above, this function is independent of t and ϕ ; therefore, p_t and p_ϕ will be the two integrals of motion, namely,

$$\dot{\phi} = \frac{L}{h(r)} \quad \dot{t} = \frac{E}{f(r)}.$$

Now for the general form of Hamiltonian, we have

$$\Pi = \dot{x}^\mu p_\mu - \mathcal{L} = \Delta,$$

where $\Delta = 1, 0$ for time-like and null geodesics. Here, we consider a four-momentum and Hamiltonian condition for null geodesics:

$$\Pi = \frac{p^\nu p^\mu g_{\mu\nu}}{2} = 0, \quad (9)$$

the radial component of the null geodesic equations will be [25]

$$\dot{r}^2 + V_{\text{eff}} = 0, \quad (10)$$

and

$$V_{\text{eff}} = g(r) \left(\frac{L^2}{h(r)} - \frac{E^2}{f(r)} \right), \quad (11)$$

where E and L represent the photon's energy and total angular momentum, respectively. A circular null geodesic occurs at an extremum of the effective potential $V_{\text{eff}}(r)$, which is given by

$$V_{\text{eff}} = 0, \quad \partial_r V_{\text{eff}} = 0. \quad (12)$$

These local extrema of the effective potential are equivalent to unstable and stable circular null geodesics, which correspond to a photon sphere and an anti-photon sphere. By considering the equations (12) simultaneously, we obtain following expression:

$$\left(\frac{f(r)}{h(r)} \right)'_{r=r_{ps}} = 0, \quad (13)$$

where the prime is the derivative with respect to r . By re-writing (13), we obtain

$$f(r)h(r)' - f(r)'h(r) = 0. \quad (14)$$

The first term at the horizon will be disappear, but the second term typically remains non-zero, meaning that r_{ps} and r_h do not coincide. According to the results and concepts of the above discussion, we can now investigate the topological characteristics of the photon sphere.

We begin this work by introducing a regular potential [6]:

$$H(r, \theta) = \sqrt{\frac{-g_{tt}}{g_{\varphi\varphi}}} = \frac{1}{\sin\theta} \left(\frac{f(r)}{h(r)} \right)^{1/2}, \quad (15)$$

The discussion of this potential enables us to search for the radius of our photon sphere at

$$\partial_r H = 0$$

Therefore, we can use a vector field $\phi = (\phi^r, \phi^\theta)$,

$$\phi^r = \frac{\partial_r H}{\sqrt{g_{rr}}} = \sqrt{g(r)} \partial_r H, \quad \phi^\theta = \frac{\partial_\theta H}{\sqrt{g_{\theta\theta}}} = \frac{\partial_\theta H}{\sqrt{h(r)}}. \quad (16)$$

With the above definition ϕ , and recalling the relationships of Duan's section, we now define the current and charge (3) for this new potential.

Furthermore, based on relation (7) and the distinctive properties of the Dirac delta function, we can infer that the charges will manifest as non-zero exclusively at the

loci where ϕ vanishes. The photon sphere is located precisely at these junctures, thereby enabling the assignment of a topological charge Q to each photon sphere. Pursuant to Eq. (7), upon considering Ω as a manifold encompassing a singular zero point, subsequent analysis reveals that Q is precisely commensurate with the winding number. Let C_i denote a closed, smooth, and positively oriented curve that encapsulates solely the i_{th} zero point of ϕ , while all other zero points lie external to it. Thus, the winding number can be calculated using the following formula:

$$\omega_i = \frac{1}{2\pi} \oint_{C_i} d\Lambda, \quad (17)$$

where Λ is

$$\Lambda = \frac{\phi^2}{\phi^1}, \quad (18)$$

then the total charge will be

$$Q = \sum_i \omega_i. \quad (19)$$

In conclusion, when the closed curve encompasses a zero point, Q is precisely equivalent to the winding number. In instances where the curve encloses multiple zero points, Q will be the aggregate of the winding numbers corresponding to each zero point. Conversely, if the curve circumscribes no zero points, the resultant charge must invariably be zero.

III. EXPLANATION OF TOPOLOGICAL CHARGES BASED ON PROPERTIES OF THE EFFECTIVE POTENTIAL

Before delving into further details, perhaps the most important question to address is, What insights can the study of different photon sphere structures provide regarding the nature of black holes? Note that the stability/instability of photon orbits around black holes plays a crucial role in shaping the observed black hole shadow and can provide insights into the presence of naked singularities. The shadow of a black hole is essentially the silhouette created by the event horizon against the backdrop of light from the accretion disk or other sources. The shape and size of this shadow are influenced by the photon orbits, which are paths that light can take around the black hole. The EHT's observations of M87* and Sgr A* provide invaluable data on black hole shadows. These observations confirm the predictions of stable orbits affecting the shape and size of the shadow. The amount of light that visibly circles the black hole and

contributes to its shadow can provide insights into the structure surrounding it, potentially revealing the presence of an accretion disk, which influences photon paths [30]. For a non-rotating black hole, the shadow is nearly circular. However, for a rotating black hole, the shadow becomes distorted owing to frame-dragging effects, where space-time itself is twisted by the black hole's rotation [31]. The size of the shadow is determined by the radius of the photon sphere. A larger photon sphere results in a larger shadow. If photon orbits were stable, the shadow would be more sharply defined because photons would orbit the black hole for longer periods before either escaping or being captured [32]. In reality, the orbits are unstable, leading to a more diffuse shadow boundary. This instability causes the photons to either spiral into the black hole or escape, contributing to the characteristic "fuzzy" edge of the shadow [33]. However, the scenario for the naked singularity is completely different. Naked singularities, if they exist, would present a very different observational signature from black holes. The lack of an event horizon means that photons could potentially orbit much closer to the singularity, leading to more extreme bending of light and potentially observable differences in the light patterns. This would lead to unique gravitational lensing effects, where light from background stars or other objects would be bent in unusual ways. In these cases, instead of well-defined shadows, we might expect unique visual signatures, such as anomalously bright phenomena formed by gravitational lensing effects or different patterns of light emissions owing to their unstable nature [34].

In his paper, Wei demonstrated through the examination of winding numbers and the calculation of total charges for a model that whenever the TTC is -1 , the structure will exhibit black hole behavior; conversely, if the TTC is 0 , the structure will be in the form of a naked singularity [25]. We have extended this work to show that in addition to the value of 0 , a TTC value of $+1$ can also appear as a naked singularity [26]. In addition to utilizing the aforementioned analysis and topological charge analysis to classify the behavior of the studied structure and determine its parameter ranges, in this paper, we examine the geometric behavior of the effective potential (15), which exhibits precise alignment with the topological charges. A significant and distinct aspect of this potential, compared with traditional potentials used for studying photon spheres and null geodesics, is that it is independent of the energy and angular momentum of the incoming particle. This implies that this potential is an inherent property of the spacetime structure. Our observations in multiple cases [35–37] indicate that when the studied system exhibits a topological charge of -1 , it always has the event horizon and exhibits black hole behavior. In such a scenario, the potential function reveals a dominant maximum outside the event horizon, indicating instability at

the photon sphere location. Conversely, when the ultra-compact object under study exhibits a topological charge of 0 or +1, the system generally lacks an event horizon and takes the form of a naked singularity. In this case, the potential function exhibits a dominant minimum alongside the maximum, indicating the presence of a stable photon sphere. An important and intriguing point should be indicated here. From a classical perspective, the existence of a minimum energy state (stable condition) alongside a maximum energy state (unstable condition) implies that the system will naturally and spontaneously move towards the stable minimum. Consequently, the emergence of a stable photon sphere in proximity to an unstable photon sphere may cause any photon capable of leaving the unstable maximum to be absorbed by the nearest stable minimum. This suggests that the spacetime in question should be considered "off" from the perspective of observation and information reception.

Before discussing the main models and for a better understanding of each of the topological states stated above, we use an example separately below.

Case I: TTC = -1

Typically, in such a scenario, one or several zero points emerge outside the event horizon in a manner that maintains the total charges at -1, and the structure with the unstable photon sphere remains in the form of a black hole.

As observed in Fig. 1(a), this black hole has a single zero point outside its event horizon, resulting in a TTC of -1, corresponding with reference [25]. In Fig. 1(b), we have plotted the potential $H(r)$. We can observe that this potential has a global maximum, which, upon closer inspection of Fig. 1(c), is precisely located at the zero point

or, in other words, at the same location as the photon sphere. As this point represents a global maximum, any photon trapped within this potential will abandon this peak at the slightest disturbance, in pursuit of a state with lower energy. This signifies that we have an unstable photon sphere, precisely the phenomenon of observational interest.

Case II: TTC = 0 or +1

From an energy perspective, these two states occur when one or more local or global minima appear in the studied spacetime. For the topological charge 0 case, as observed in Fig. 2(b), a minimum (a stable photon sphere) at $r = 1.389900878$ can be clearly observed adjacent to a maximum (an unstable photon sphere). We must note a few points here. First, this state typically occurs when, from the metric function's perspective, we are in a rootless region, without a horizon, or in a space termed as a naked singularity. In other words, although these minima have always existed, even in the black hole state, their influence on the final outcome only becomes apparent when the event horizon has disappeared, which equates to a naked singularity for an ultra-compact object. Second, we must consider whether the structural influence in the form of a naked singularity is unlimited. The answer depends on the model under study; occasionally, parametric conditions occur where neither the metric nor potential function has a solution for the studied interval. In other words, beyond that parametric range, neither the metric nor potential function practically provides a solution for the space, which we refer to as the forbidden region.

In Fig. 3, we encounter a scenario with a TTC of +1. Here, more than one minimum appears in the studied

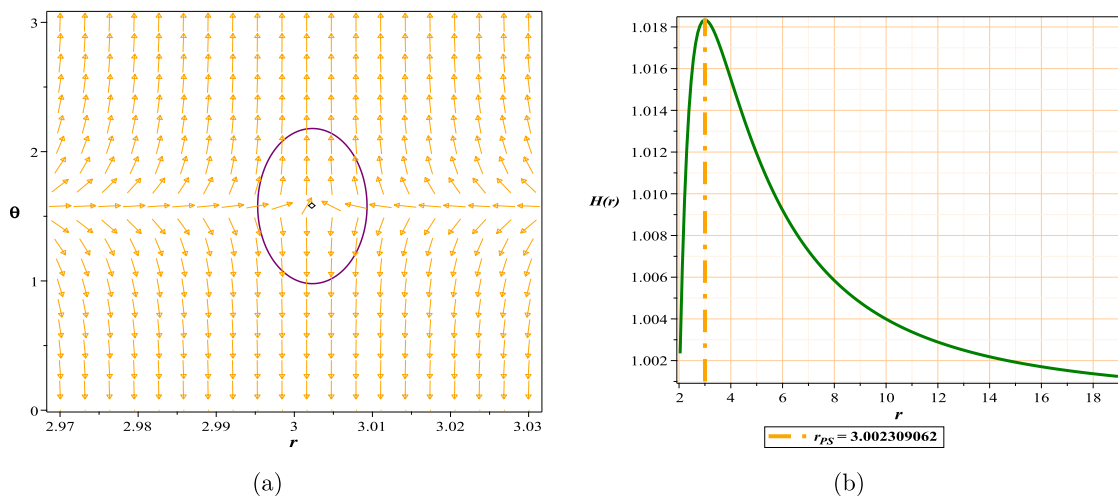


Fig. 1. (color online) (a) Normal vector field n in the $(r-\theta)$ plane, the photon sphere is located at $(r, \theta) = (3.002309062, 1.57)$ with respect to $(g = -0.21834, m = 1, l = 1)$; (b) topological potential $H(r)$ for the regular Hayward AdS black hole model.

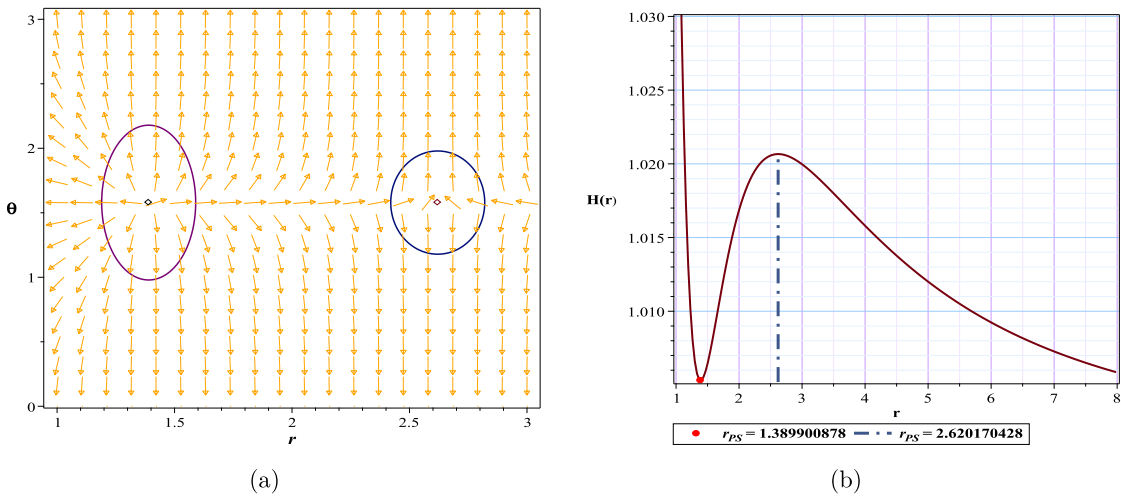


Fig. 2. (color online) (a) Normal vector field n in the $(r-\theta)$ plane, the photon spheres are located at $(r, \theta) = (1.389900878, 1.57)$ and $(r, \theta) = (2.620170428, 1.57)$ with respect to $(g = 1.08, m = 1, l = 1)$; (b) topological potential $H(r)$ for the regular Hayward AdS black hole model.

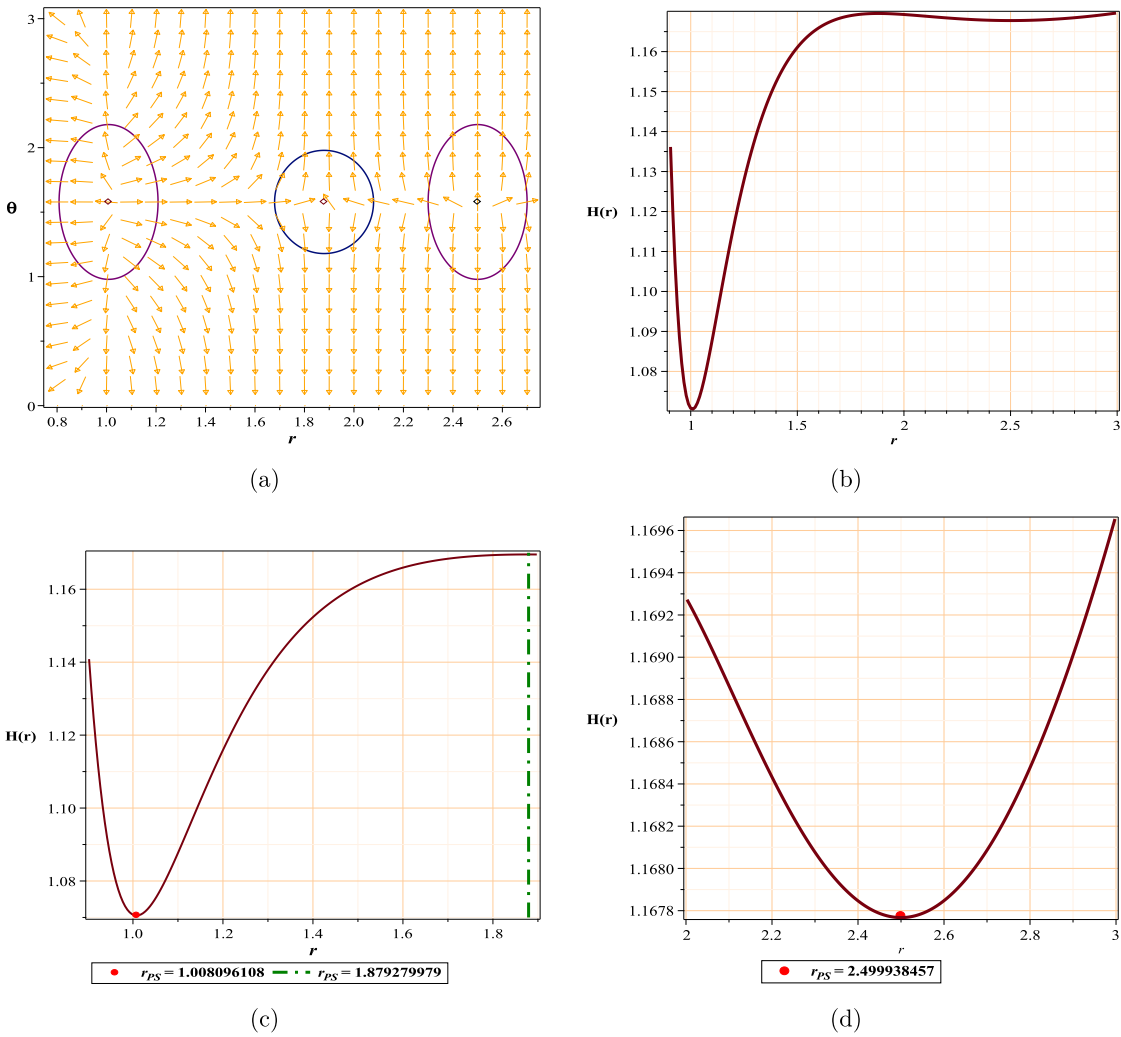


Fig. 3. (color online) (a) PSs located at $(r-\theta) = (2.499938457, 1.57)$, $(r-\theta) = (1.879279979, 1.57)$, $(r-\theta) = (1.008096108, 1.57)$ with respect to $(q = 0.9, z = 1.1, M = 1.6, \theta = 0)$; (b) topological potential $H(r)$ for the hyperscaling violating model, (c), (d) enlarged details of diagram (b).

space-time.

IV. EFFECTIVE POTENTIAL AND TOPOLOGICAL PHOTON SPHERES AS A TOOL FOR CLASSIFICATION

Before we discuss the selected models, we briefly compare the advantages and disadvantages of this method relative to the traditional approach. In the traditional approach to studying photon spheres, the Lagrangian must be extracted from the action; subsequently, the Hamiltonian is constructed. When the Hamiltonian is determined, the effective potential can be constructed, which enables the study of the photon sphere. This potential is a function of the energy and angular momentum of the particle.

A notable advantage of this method is the direct use of the metric function to construct the potential, bypassing all the aforementioned steps. Additionally, the resulting potential is independent of the parameters of the incoming particle and is solely a function of the surrounding spacetime geometry. Using the equatorial plane for the vector field (ϕ), similar to the Poincaré plane, and the resulting dimensional reduction, is another significant advantage. Ultimately, the ability to study a broader range of the space surrounding an ultra-compact object is a fundamental aspect that, for the first time, leads to the classification of different spacetime regions based on this method. Finally, this method enables the introduction of a practical concept, which we term the possible radius limit for the photon sphere.

R_{PLPS} : Considering the permissible parameter range to maintain the black hole structure, we define the minimum or maximum possible radius for the appearance of an unstable photon sphere as R_{PLPS} .

However, some fundamental limitations must be considered. Because the vector field (ϕ) must be separable with respect to spatial coordinates, only diagonal metrics with spherical symmetry can be used. Because most models of interest have spherical structures and the others can often be expressed diagonally using the C -metric, this limitation can be somewhat ignored. Another problem is that because the Poincaré plane is used for dimensional reduction, this method may not be applicable to models with fewer than four dimensions. Finally, as this is a nascent approach, weaknesses may exist that become apparent over time. Interestingly, the simplifications, computational power, and novelty of this method and mathematical model for studying symmetric potential functions have attracted such interest that the mathematical structure of the model has been extended to thermodynamics. Consequently, extensive studies based on the mathematical model of this method have been conducted on the phase

transitions of black hole models [38–55].

A. Photon Sphere and perfect fluid dark matter black hole (PFDM)

Cosmological calculations show that the surrounding universe contains 73% dark energy, 23% dark matter, and the remainder consisting of baryonic matter [56–58]. This has been confirmed, to some extent, using baryonic sound oscillations, cosmic microwave background, weak lensing, and other methods. Additionally, astrophysical observations show that massive black holes, surrounded by enormous halos of dark matter, are located in the centers of giant spiral and elliptical galaxies. These evidences can be acceptable reasons for the fact that we should give more attention to black hole solutions in the presence of dark matter and dark energy [59–64]. For this purpose, we select the four-dimensional PFDM model [65], whose metric is

$$f = 1 - \frac{2M}{r} - \frac{\lambda \ln\left(\frac{r}{\lambda}\right)}{r}, \quad (20)$$

where M is mass, and λ is the parameter of intensity of PFDM. Additionally, we have

$$f(r) = g(r), \quad (21)$$

$$h(r) = r. \quad (22)$$

From Eq. (15) for potential and with respect to the above equations, we have

$$H = \frac{\sqrt{1 - \frac{2M}{r} - \frac{\lambda \ln\left(\frac{r}{\lambda}\right)}{r}}}{\sin(\theta)r}. \quad (23)$$

With respect to Eqs. (21) and (22) and from Eq. (16), we have

$$\phi^r = \frac{\left(3 \ln\left(\frac{r}{\lambda}\right) \lambda + 6M - 2r - \lambda\right) \csc(\theta)}{2r^3}, \quad (24)$$

$$\phi^\theta = -\frac{\sqrt{1 - \frac{2M}{r} - \frac{\lambda \ln\left(\frac{r}{\lambda}\right)}{r}} \cos(\theta)}{\sin(\theta)^2 r^2}. \quad (25)$$

In the first case (Case I: $TTC = -1$), considering the selected value of the parameter $\lambda = 0.62$ and the presence of the event horizon ($r_h = 2.97163$) (Fig. 4), we observe the appearance of a photon sphere outside the event horizon.

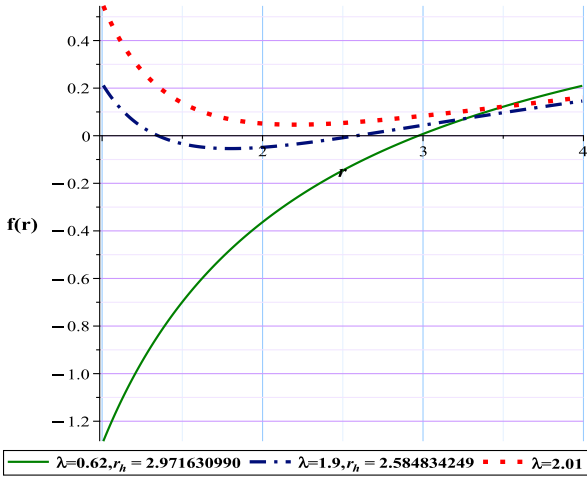


Fig. 4. (color online) Metric function with different λ for the PFDM black hole model.

This photon sphere has a topological charge of -1 (Fig. 5(a)) and, as evident in Fig. 5(b), represents an energy maximum. Consequently, in this case, we are confronted with a black hole that contains an unstable photon sphere. However, in the second case (Case II: TTC = 0), our choice of $\lambda = 2.15$ results in a metric function without roots, which is clearly visible in Fig. 4. The gravitational structure exhibits two photon spheres with charges of -1 and $+1$, indicating a space-time with a TTC of zero (Fig. 6(a)). Energy-wise, this scenario is equivalent to the emergence of both a minimum and maximum, as shown in Fig. 6(b). Given these conditions, in this scenario, the structure

manifests itself in the form of a naked singularity.

Now, we must answer the question, For what values of the parameter λ will the space be in the form of a black hole or naked singularity? We show the answers to this question in Table 1. Here, we must note that we have focused on the domain of λ and assigned an arbitrary value to M . Obviously, changing these values can change our parameter range.

B. Photon Sphere and charged AdS black hole with perfect fluid dark matter (CPFDM)

To observe the effects of adding the electric field and the AdS radius to the action of the PDFM model on the sphere-topological photon structure, this time we use the CPFDM model in the AdS form [66]. The metric for such black hole is

$$f(r) = 1 - \frac{2m}{r} + \frac{q^2}{r^2} + \frac{r^2}{l^2} + \frac{\ln\left(\frac{r}{\lambda}\right)\lambda}{r}, \quad (26)$$

where m is mass, q is charge, λ is the parameter of intensity of PFDM, and l is the AdS radius length.

With respect to Eqs. (21) and (22) and from Eqs. (15) and (16), we have

$$H = \frac{\sqrt{1 - \frac{2m}{r} + \frac{q^2}{r^2} + \frac{r^2}{l^2} + \frac{\ln\left(\frac{r}{\lambda}\right)\lambda}{r}}}{\sin(\theta)r}, \quad (27)$$

$$\phi^r = \frac{\left(-3 \ln\left(\frac{r}{\lambda}\right)\lambda r - 2r^2 + (6m + \lambda)r - 4q^2\right) \sqrt{1 - \frac{2m}{r} + \frac{q^2}{r^2} + \frac{r^2}{l^2} + \frac{\ln\left(\frac{r}{\lambda}\right)\lambda}{r}}}{2 \sqrt{\frac{\ln\left(\frac{r}{\lambda}\right)\lambda r l^2 + (-2mr + q^2 + r^2)l^2 + r^4}{r^2 l^2}} r^4 \sin(\theta)}, \quad (28)$$

$$\phi^\theta = -\frac{\sqrt{1 - \frac{2m}{r} + \frac{q^2}{r^2} + \frac{r^2}{l^2} + \frac{\ln\left(\frac{r}{\lambda}\right)\lambda}{r}} \cos(\theta)}{\sin(\theta)^2 r^2}. \quad (29)$$

Here, we have focused on λ and assigned arbitrary values to m , l , and q . We clearly observe that changing these values can cause a change in our parameter range.

Table 2 shows that the forbidden regions are located next to the allowed regions, and this black hole has practically no region that is equivalent to the naked singularity in terms of total topological charges. As shown in Fig. 7(a), the structure exhibits the behavior of a normal

black hole with a total charge of -1 and an unstable photon sphere, which is confirmed with a maximum energy (Fig. 7(b)). Compared with the results from the previous state, the addition of an electric field and AdS radius to the action appears to diminish the impact of the PDFM term. This is because changes in λ , which previously led to the emergence of energy minima beyond the event horizon and drove the model towards a naked singularity, now have no effect.

C. Photon sphere and Euler-Heisenberg black hole

The Euler-Heisenberg black hole is a type of black hole that has a nonlinear electromagnetic field due to

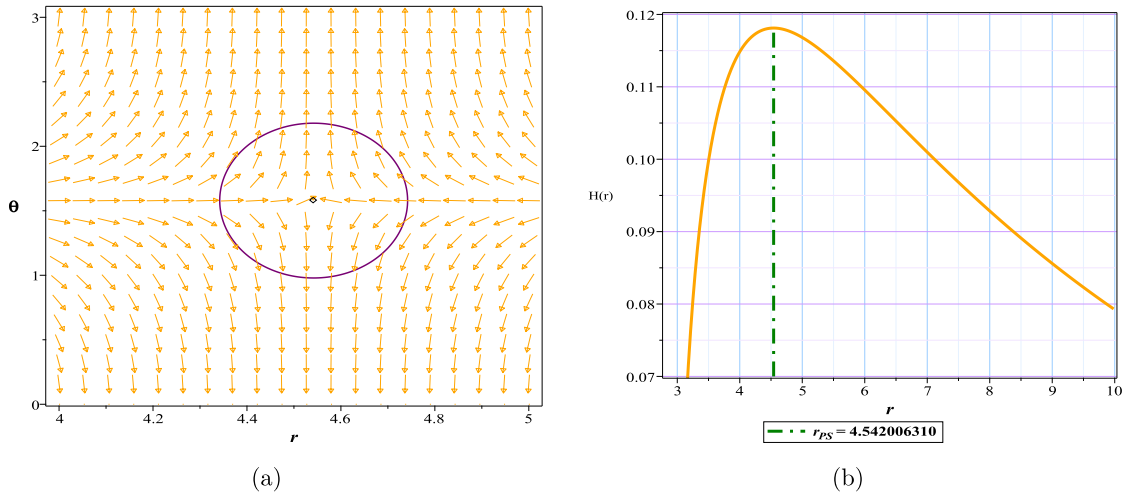


Fig. 5. (color online) (a) Normal vector field n in the $(r-\theta)$ plane, the photon sphere is located at $(r, \theta) = (4.542006310, 1.57)$ with respect to $(\lambda = 0.62, M = 1)$; (b) topological potential $H(r)$ for the PFDM black hole model.

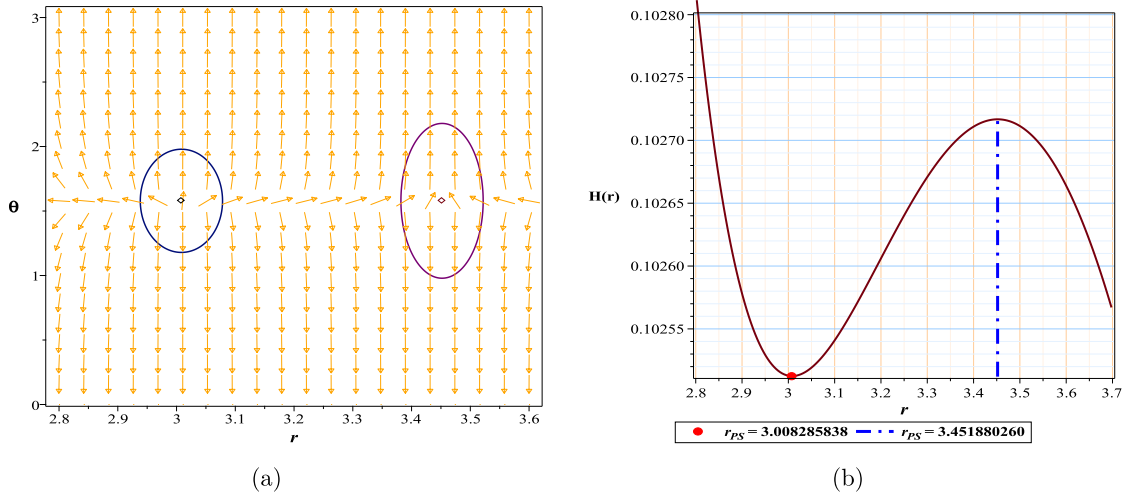


Fig. 6. (color online) (a) Normal vector field n in the $(r-\theta)$ plane, the photon spheres are located at $(r, \theta) = (3.008285838, 1.57)$ and $(r, \theta) = (3.451880260, 1.57)$ with respect to $(\lambda = 2.15, M = 1)$; (b) topological potential $H(r)$ for the PFDM black hole model.

Table 1. *Unauthorized region: the region in which the roots of ϕ equations become negative or imaginary in this region.

PFDM black holes	Fix parameters	Conditions	*TTC	(R_{PLPS})
*Unauthorized area	$M = 1$	$\lambda \leq 0, \lambda > 2.1554784$	<i>nothing</i>	-
Unstable photon sphere	$M = 1$	$0 < \lambda < 2$	-1	2.019966202
Naked singularity	$M = 1$	$2 < \lambda \leq 2.1554784$	0	-

TTC: *Total Topological Charge

Table 2. *Unauthorized region: the region in which the roots of ϕ equations become negative or imaginary in this region.

CPFDM black holes	Fix parameters	Conditions	*TTC
*Unauthorized area	$q = 0.1, m = 1, l = 1$	$\lambda < 0$	<i>nothing</i>
Unstable photon sphere	$q = 0.1, m = 1, l = 1$	$0 < \lambda$	-1

TTC: *Total Topological Charge

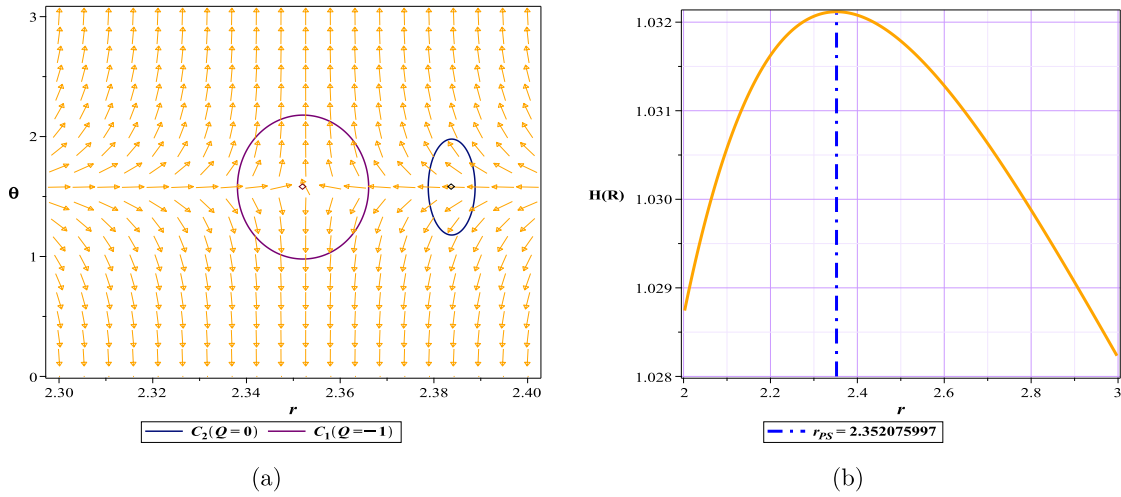


Fig. 7. (color online) Normal vector field n in the $(r-\theta)$ plane, the photon spheres are located at $(r, \theta) = (2.352075997, 1.57)$ for (a) with respect to $(q = 0.1, m = 1, \lambda = 0.2, l = 1)$; (b) topological potential $H(r)$ for the CPFDM black hole model.

quantum effects. Euler and Heisenberg developed an effective Lagrangian for quantum electrodynamics (QED) that described the interaction of photons in the presence of a strong electromagnetic field [67]. Casimir and Polder applied the Euler-Heisenberg Lagrangian to the problem of a charged black hole in general relativity. They found that QED corrections affect the electromagnetic field, thermodynamics, and stability of the black hole. They named this black hole the Euler-Heisenberg black hole and showed that it has interesting properties:

- The QED parameter, which measures the strength of the nonlinear effects, can be positive or negative. A positive QED parameter reduces the electric field near the horizon and increases the mass of the black hole, whereas a negative QED parameter enhances the electric field and decreases the mass [68].

- The QED parameter also influences the existence and location of the inner and outer horizons of the black hole. A positive QED parameter always has a single horizon, whereas a negative QED parameter can have two horizons, one horizon, or no horizon at all, depending on the values of the mass and charge [68].

- The QED parameter also modifies the stability of the black hole against perturbations. For a positive QED parameter, the black hole is stable for any mass and charge, whereas a negative QED parameter has a range of mass and charge where the black hole is unstable and can decay into radiation or smaller black holes [69].

Euler-Heisenberg's spherical four-dimensional black hole has a metric function in the following form [70]:

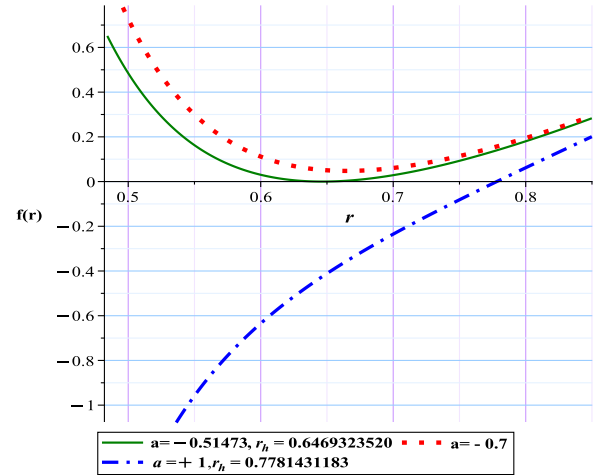


Fig. 8. (color online) Metric function with different a values for the Euler-Heisenberg black hole model.

$$f(r) = 1 - \frac{2m}{r} + \frac{q^2}{r^2} + \frac{r^2}{l^2} - \frac{aq^4}{20r^6}, \quad (30)$$

where m is the Arnowitt–Deser–Misner (ADM) mass, q is the electric charge, and a represents the strength of the QED correction. With respect to Eqs. (21) and (22) and from Eqs. (15) and (16), we have

$$H = \frac{\sqrt{100 - \frac{200m}{r} + \frac{100q^2}{r^2} + \frac{100r^2}{l^2} - \frac{5q^4a}{r^6}}}{10 \sin(\theta)r}, \quad (31)$$

$$\phi^r = \frac{(30.0r^5 - 12.8r^4 + 0.8192a - 10.0r^6) \sqrt{100 - \frac{200m}{r} + \frac{100q^2}{r^2} + \frac{100r^2}{l^2} - \frac{5q^4a}{r^6}}}{10r^8 \sin(\theta) \sqrt{\frac{(100.0r^6 - 200.0r^5 + 64.0r^4 - 2.048a) l^2 + 100.0r^8}{r^6 l^2}}}, \tag{32}$$

$$\phi^\theta = -\frac{\sqrt{\frac{(-200r^5m + 100r^4q^2 + 100r^6 - 5q^4a) l^2 + 100r^8}{l^2 r^6}} \cos(\theta)}{10 \sin(\theta)^2 r^2}. \tag{33}$$

Case I : TTC = -1

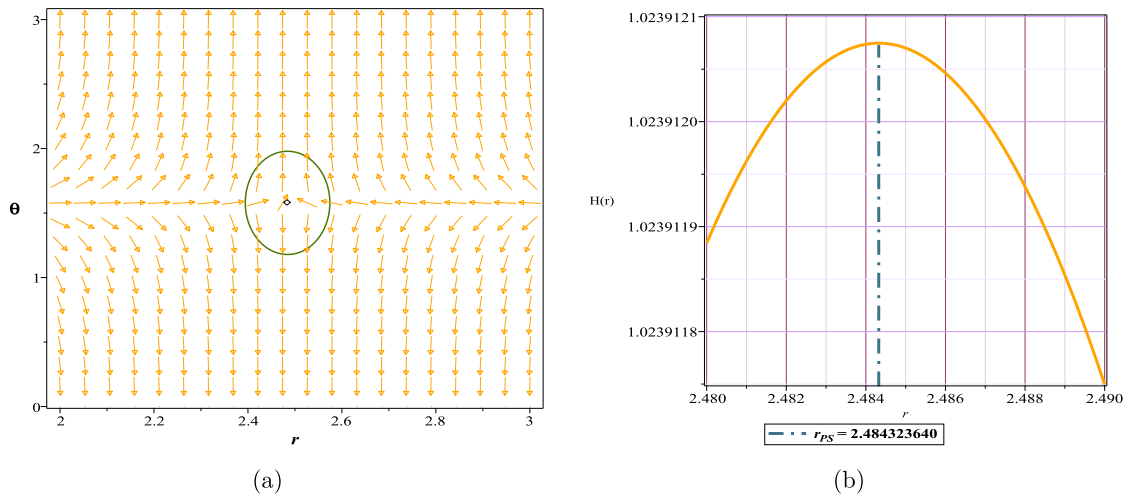


Fig. 9. (color online) Normal vector field n in the $(r-\theta)$ plane, the photon spheres are located at $(r, \theta) = (2.484328812, 1.57)$ for (a) with respect to $(q = 0.8, m = 1, a = -0.51473, l = 1)$; (b) topological potential $H(r)$ for the Euler-Heisenberg black hole model.

Case II : TTC = 0

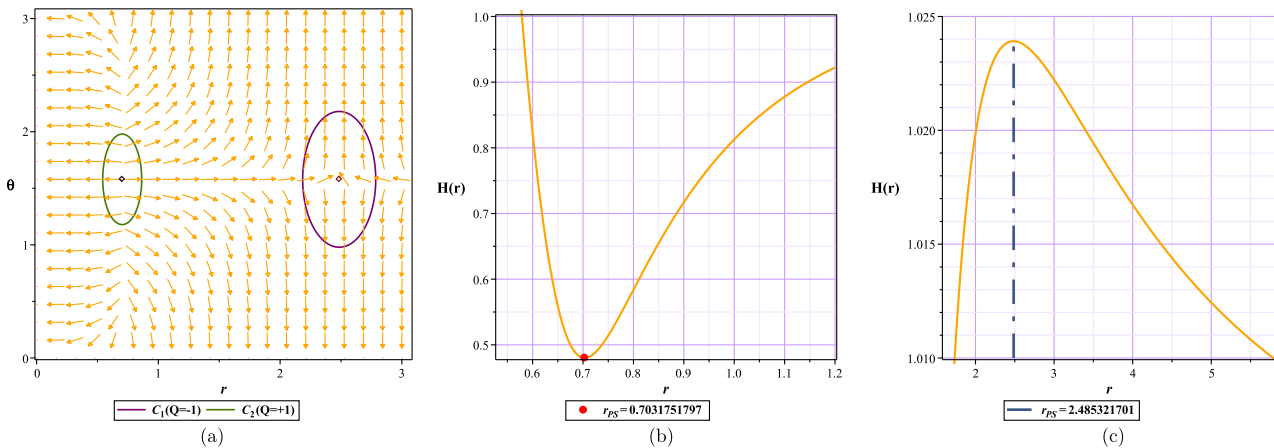


Fig. 10. (color online) Normal vector field n in the $(r-\theta)$ plane, the photon spheres are located at $(r, \theta) = (0.7031751797, 1.57)$, $(r, \theta) = (2.483792443, 1.57)$ for (a) with respect to $(q = 0.8, m = 1, a = -1, l = 1)$; (b), (c) topological potential $H(r)$ for the Euler-Heisenberg black hole model.

Table 3. *Unauthorized region: the region where the roots of ϕ equations become negative or imaginary in this region.

Euler-Heisenberg-AdS black holes	Fix parametes	Conditions	*TTC	(R_{PLPS})
*Unauthorized area	$q = 0.8, m = 1, l = 1$	$a < -144.87$	<i>nothing</i>	–
Naked singularity	$q = 0.8, m = 1, l = 1$	$-144.87 < a < -0.51473$	0	–
Unstable photon sphere	$q = 0.8, m = 1, l = 1$	$a \geq -0.51473$	–1	2.484323651

TTC: *Total Topological Charge

We have focused on parameter a ; hence, we have considered an arbitrary value for mass and charge ($m = 1, q = 0.8$). As shown in Figs. 8, 9, 10, our selected range for a can lead to different behaviors for the photon sphere. For example, Fig. 9(a), with a topological charge of -1 , indicates a normal black hole behavior, meaning that we have an unstable photon sphere. Conversely, in Fig. 10(b), the appearance of a minimum in the space without an event horizon and the zero TTC (Fig. 10(a)) all imply the existence of a naked singularity. Based on this, the following intervals can be used to obtain different modes (Table 3).

D. Photon Sphere and Euler-Heisenberg black hole surrounded by PFDM

To observe the effects of adding the PFDM to the action of the Euler-Heisenberg model on the sphere-topological photon structure, this time we use the Euler-Heisenberg black hole surrounded by PFDM [71]. The metric

$$\phi^r = -\frac{\left(15\lambda \ln\left(\frac{r}{\lambda}\right)r^5 - 5\lambda r^5 - 30m r^5 + 20q^2 r^4 + 10r^6 - 2aq^4\right) \csc(\theta)}{10r^8}, \quad (36)$$

$$\phi^\theta = -\frac{\sqrt{100 - \frac{200m}{r} + \frac{100q^2}{r^2} - \frac{5aq^4}{r^6} + \frac{100\lambda \ln\left(\frac{r}{\lambda}\right)}{r}} \cos(\theta)}{10r^2 \sin(\theta)^2}. \quad (37)$$

Case I: TTC = -1

Regardless of the impact of the AdS radius, which we have admittedly examined to a lesser extent in this article, the comparison of the results in Tables 4 and 5 with Table 3 shows that the addition of PFDM to the model has caused a significant increase in the range affected by black hole behavior. Given the negative value of a , which signifies a greater influence of the electric field, when dark matter is absent from the model (as shown in Table 3), even very small values of a rapidly expand the domain of gravitational dominance. Consequently, a gravitational minimum emerges swiftly beyond the event horizon, leading to the model becoming a naked singularity.

for this black hole is

$$f = 1 - \frac{2m}{r} + \frac{q^2}{r^2} - \frac{aq^4}{20r^6} + \frac{\lambda \ln\left(\frac{r}{\lambda}\right)}{r}, \quad (34)$$

where m is the ADM mass, q is the electric charge, λ is the parameter of intensity of PFDM, and a represents the strength of the QED correction. The behavior of the metric for different values of a is shown in Fig. 11. With respect to Eqs. (21) and (22) and from Eqs. (15) and (16), we have

$$H = \frac{\sqrt{100 - \frac{200m}{r} + \frac{100q^2}{r^2} - \frac{5aq^4}{r^6} + \frac{100\lambda \ln\left(\frac{r}{\lambda}\right)}{r}}}{10r \sin(\theta)}, \quad (35)$$

As observed in Table 3, the domain of dominance of this naked singularity is significantly extensive owing to the increase in the parameter within a considerably large negative range. However, in the presence of dark matter (as indicated in Tables 4 and 5), this structure appears to act as a reverse agent, preventing the rapid growth and expansion of the model's gravitational domain. Thus, as evident, we maintain the conditions for the existence of a black hole with an unstable photon sphere over a large range of negative a values. In other words, the inclusion of dark matter appears to somewhat prevent the formation of gravitational minima over a larger range, which is an intriguing effect.

Case II: TTC = 0

E. Photon sphere and black holes with nonlinear electrodynamics (NLE)

The concept that nonlinear electrodynamics might be

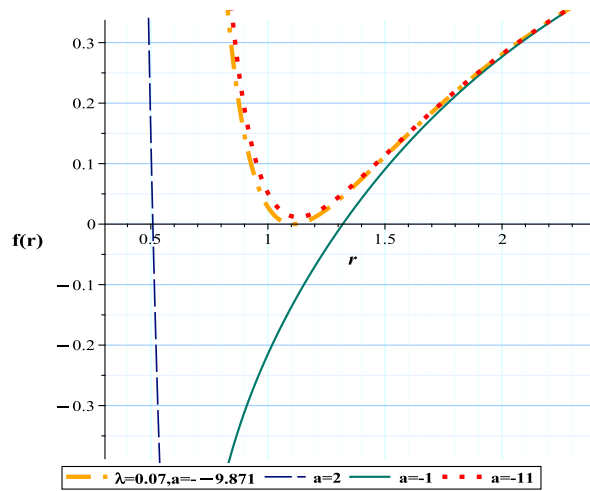


Fig. 11. (color online) Metric function with different a values for the Euler-Heisenberg black hole surrounded by PFDM.

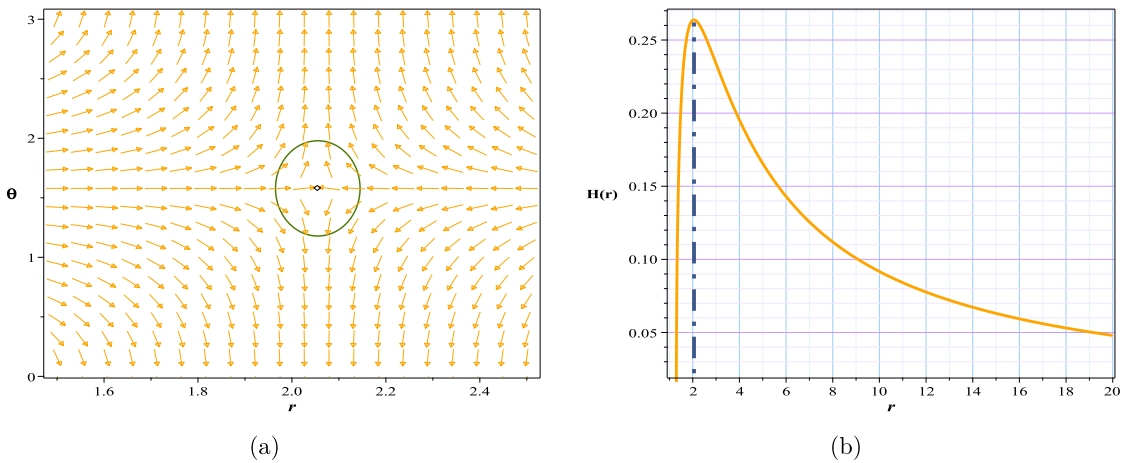


Fig. 12. (color online) Normal vector field n in the $(r-\theta)$ plane, the photon spheres are located at $(r, \theta) = (2.055057, 1.57)$ for (a) with respect to $(q = 0.8, m = 1, a = -0.51473, l = 1, \lambda = 0.07)$; (b) topological potential $H(r)$ for the Euler-Heisenberg black hole surrounded by PFDM.

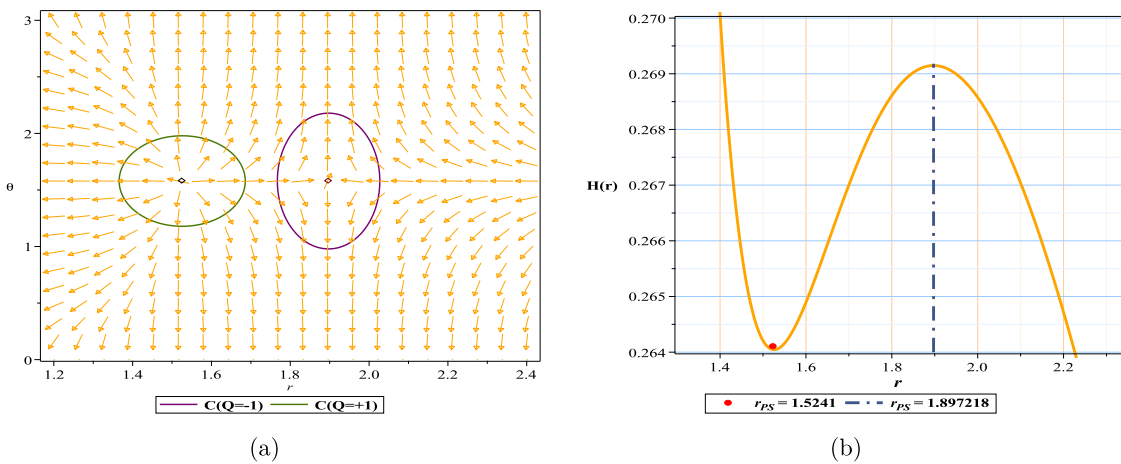


Fig. 13. (color online) Normal vector field n in the $(r-\theta)$ plane, the photon spheres are located at $(r, \theta) = (1.5241, 1.57)$, $(r, \theta) = (1.897218, 1.57)$ for (a) with respect to $(q = 0.8, m = 1, a = -1, l = 1, \lambda = 0.07)$; (b) topological potential $H(r)$ for the Euler-Heisenberg black hole surrounded by PFDM.

Table 4. *Unauthorized region: the region in which the roots of ϕ equations become negative or imaginary in this region.

Euler-Heisenberg PFDM black holes	Fix parametes	Conditions	*TTC	(R_{PLPS})
*Unauthorized area	$q = 0.8, m = 1, \lambda = 0.07$	$a < -40$	<i>nothing</i>	-
Naked singularity	$q = 0.8, m = 1, \lambda = 0.07$	$-39 \leq a < -9.872$	0	-
Unstable photon sphere	$q = 0.8, m = 1, \lambda = 0.07$	$a \geq -9.871$	-1	2.026241903

TTC: *Total Topological Charge

Table 5. *Unauthorized region: the region in which the roots of ϕ equations become negative or imaginary in this region.

Euler-Heisenberg PFDM black holes	Fix parametes	Conditions	*TTC	(R_{PLPS})
*Unauthorized area	$q = 0.8, m = 1, \lambda = 0.6$	$a < -14.9$	<i>nothing</i>	-
Naked singularity	$q = 0.8, m = 1, \lambda = 0.6$	$-14.9 < a < -4.21$	0	-
Unstable photon sphere	$q = 0.8, m = 1, \lambda = 0.6$	$a \geq -4.2$	-1	1.583699320

TTC: *Total Topological Charge

solve the problem of black hole singularities led to many studies to determine regular solutions, which led to black holes such as "Bardeen" [72] or "Ayon-Beat-Garcia" [73, 74]. For the last model we select for our research, we use a black hole that was selected by Gao [75] to investigate the effects of nonlinear electrodynamics and the possibility that a black hole can have more than two event horizons.

We study this black hole in three- and four-horizon states, and we show that additional studies confirm the results of the mentioned article in three-horizon states.

Three – Horizons mode

Therefore, according to [75] for the metric function in

the case of three horizons, we have

$$f = 1 - \frac{2m}{r} + \frac{q^2}{r^2} + \frac{2q^4\alpha_2}{5r^6}, \tag{38}$$

where α_2 represents dimensional constants, m is mass, and q is charge. The behavior of the metric for different values of α_2 is shown in Fig. 14. With respect to Eqs. (21) and (22) and from Eqs. (15) and (16), we have

$$H = \frac{\sqrt{25 - \frac{50M}{r} + \frac{25q^2}{r^2} + \frac{10q^4\alpha_2}{r^6}}}{5 \sin(\theta) r}, \tag{39}$$

$$\phi^r = \frac{(15Mr^5 - 10q^2r^4 - 5r^6 - 8q^4\alpha_2) \sqrt{25 - \frac{50M}{r} + \frac{25q^2}{r^2} + \frac{10q^4\alpha_2}{r^6}}}{5 \sqrt{\frac{-50Mr^5 + 25q^2r^4 + 25r^6 + 10q^4\alpha_2}{r^6}} r^8 \sin(\theta)}, \tag{40}$$

$$\phi^\theta = -\frac{\sqrt{25 - \frac{50M}{r} + \frac{25q^2}{r^2} + \frac{10q^4\alpha_2}{r^6}} \cos(\theta)}{5 \sin(\theta)^2 r^2}. \tag{41}$$

The results of Gao's work on the black hole showed that to have three horizons, we require $\alpha_2 < 0$. Note that our results confirm the above-mentioned limit for black hole behavior. Our results show that for $\alpha_2 \leq 4.8148$, the model exhibits the behavior of a regular black hole and has an unstable photon sphere, Fig. 6(a). For the range $4.8148 < \alpha_2 < 18.1064$, the behavior of the model is the

naked singularity (Fig. 6(b)), and for a limit greater than that, the system lacks any spherical photon structure, either stable or unstable, and practically, it will most likely lack a black hole structure (Table 6). Because the structure of the energy diagrams is similar to the previous behaviors, we have refrained from displaying them here.

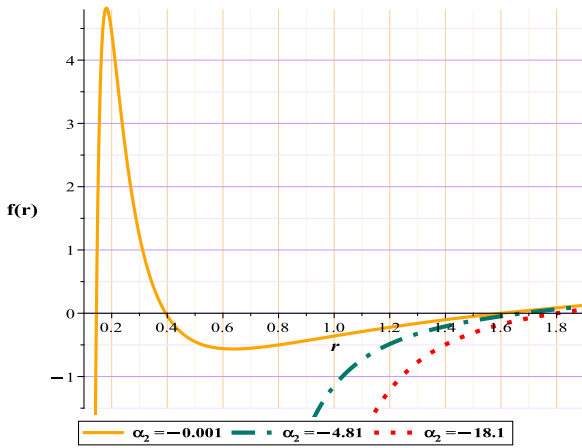


Fig. 14. (color online) Metric function with different α for NLE model.

Four – Horizons mode

Unlike all previous shapes, in this case, another parameter has been added to our equations. This means that, because we have only one condition to establish, our restrictions are increased, and we must provide a value to one of the parameters and add it to our constants table.

According to [75] for the metric function in the case of four horizons, we have

$$f(r) = 1 - \frac{2m}{r^2} + \frac{q^2}{r^2} + \frac{2q^4\alpha_2}{5r^6} + \frac{q^6(16\alpha_2^2 - 4\alpha_3)}{9r^{10}}, \quad (42)$$

where α_i denotes dimensional constants, m is the mass, and q is the charge. With respect to Eqs. (21) and (22) and from Eqs. (15) and (16), we have

$$H = \frac{\sqrt{225 - \frac{450m}{r^2} + \frac{225q^2}{r^2} + \frac{90q^4\alpha_2}{r^6} + \frac{25q^6(16\alpha_2^2 - 4\alpha_3)}{r^{10}}}}{15 \sin(\theta) r}, \quad (43)$$

$$\phi^r = \frac{-15r^{10} + (-30q^2 + 60m)r^8 - 24q^4\alpha_2r^4 - 160q^6\left(\alpha_2^2 - \frac{\alpha_3}{4}\right)}{15r^{12} \sin(\theta)}, \quad (44)$$

$$\phi^\theta = -\frac{\sqrt{225 - \frac{450m}{r^2} + \frac{225q^2}{r^2} + \frac{90q^4\alpha_2}{r^6} + \frac{25q^6(16\alpha_2^2 - 4\alpha_3)}{r^{10}}}}{15 \sin(\theta)^2 r^2} \cos(\theta). \quad (45)$$

V. CONCLUSIONS

Given the necessity of photon rings and photon spheres for gravitational structures in numerous studies [15–20, 76–88], this article presents a new approach for determining parameter ranges in ultra-compact gravitational objects using topological charges and behavioral patterns associated with photon spheres. To achieve this, we examine models often influenced by PDFM and, in one case, a model with multiple horizons. We meticulously plot field diagrams, zero points, total topological charges, and effective potential diagrams. Based on these results, we provide a detailed classification of the behavior and characteristics of each model in terms of gravitational influence on photon motion, as shown in Tables 1–7. To better understand the obtained results, we compare the results presented in the tables before summarizing the overall findings. As a comparison of Tables 1 and 2 shows, in the PDFM black hole, the parameter Λ only

causes the model to assume the form of a black hole within the range of 0 to 2. However, the addition of a charge and the AdS radius completely alters this range, such that the model no longer exhibits the form of a naked singularity within the studied values. This behavioral difference, which results solely from the addition of electric fields to the model, can be quite intriguing. In contrast, in the Euler-Heisenberg model, the results appear to be clearer. As shown in Table 3, within a wide range of negative a values, the structure has the form of a naked singularity, and only within a small range of negative a values does the structure maintain the form of a black hole. Adding PDFM to the model in this case significantly reduces the range of naked singularity and enables more negative values to maintain the model in the form of a black hole. As negative a values can indicate the presence of repulsive interactions that counteract the usual attractive gravitational effects, if the model reaches an extremal or super-extremal state under certain conditions, it

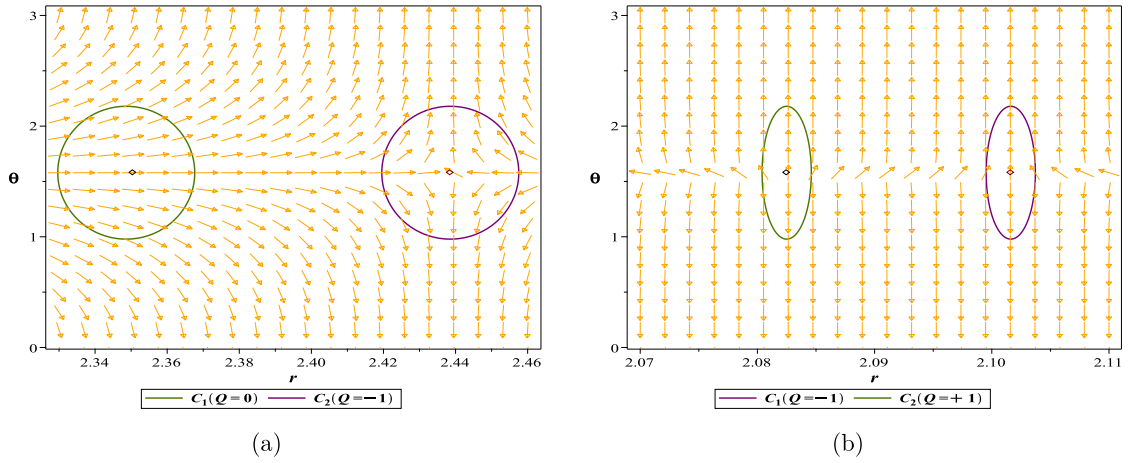


Fig. 15. (color online) Normal vector field n in the $(r-\theta)$ plane, the photon spheres are located at $(r, \theta) = (2.438537647, 1.57)$ for (a) with respect to $(q = 0.8, m = 1, \alpha_2 = -4.81)$ and $(r, \theta) = (2.082498057, 1.57)$; $(r, \theta) = (2.101619064, 1.57)$ for (b) with respect to $(q = 0.8, m = 1, \alpha_2 = -18.1)$.

Table 6. *Unauthorized region: the region in which the roots of ϕ equations become negative or imaginary in this region.

NLE black holes (three-horizon mode)	Fix parametes	Conditions	*TTC	(R_{PLPS})
Unstable photon sphere	$q = 0.8, m = 1$	$\alpha_2 \leq 4.8148$	-1	2.438486243
Naked singularity	$q = 0.8, m = 1$	$4.8148 < \alpha_2 < 18.1064$	0	-
*Unauthorized area	$q = 0.1, m = 8$	$18.1064 < \alpha_2$	nothing	-

TTC: *Total Topological Charge

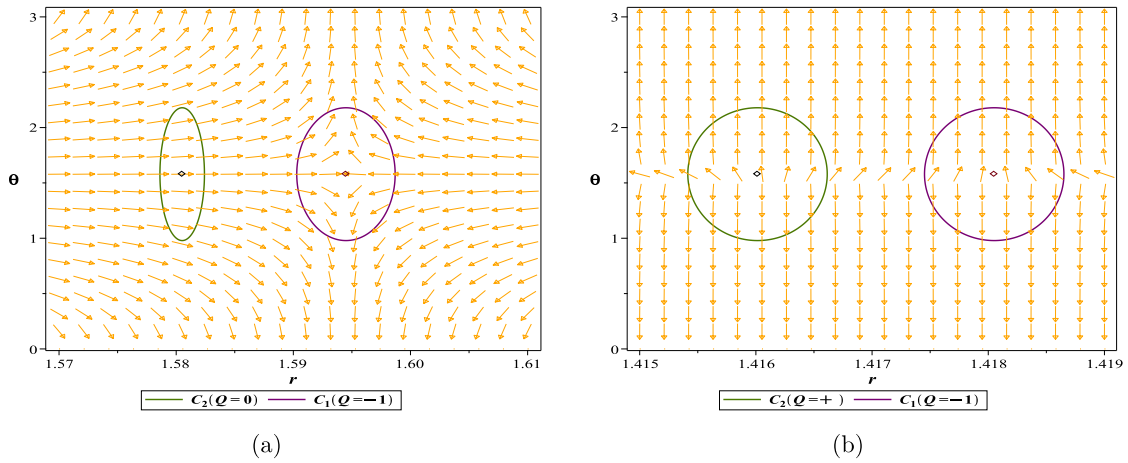


Fig. 16. (color online) Normal vector field n in the $(r-\theta)$ plane, the photon spheres are located at $(r, \theta) = (1.594492202, 1.57)$ for (a) with respect to $(q = 0.9, m = 1, \alpha_2 = -1, \alpha_3 = 4)$ and $(r, \theta) = (1.416014166, 1.57)$; $(r, \theta) = (1.418051264, 1.57)$ for (b) with respect to $(q = 0.9, m = 1, \alpha_2 = -1, \alpha_3 = -3.2541)$.

Table 7. *Unauthorized region: the region where the roots of ϕ equations become negative or imaginary in this region.

NLE black holes (four-horizon mode)	Fix parametes	Conditions	*TTC	(R_{PLPS})
*Unauthorized area	$q = 0.9, m = 1, \alpha_2 = -1$	$\alpha_3 < -3.2543$	nothing	-
Naked singularity	$q = 0.9, m = 1, \alpha_2 = -1$	$-3.2543 < \alpha_3 < 3.99$	0	-
Unstable photon sphere	$q = 0.9, m = 1, \alpha_2 = -1$	$4 \leq \alpha_3$	-1	1.594492202

TTC: *Total Topological Charge

would provide suitable conditions for the formation of the Weak Gravity Conjecture (WGC). Note that although the obtained ranges may not all have physical significance, and to have a fully physical range, they must be interpreted alongside conditions such as energy conditions. However, the mutual influence of parameters and the regions in which photon spheres appear can clearly serve as a significant criterion for studying the model's behavior. This reciprocal relationship between the photon sphere and gravitational structure is an ideal advantage, and studying it from both perspectives can lead to several interesting outcomes:

- As an initial result, calculating the location of photon spheres, interpreting their topological charge, and determining the effective gravitational range on photon motion (black hole and naked singularity) can serve as a new approach, motivating a further study of various models based on this method. For instance, in this study, we observe that an unstable photon sphere, equivalent to the presence of an unstable maximum in the potential function, only appears in the spacetime influenced by the model when an event horizon exists. Therefore, based on these results and similar experiences [35, 89, 90], one of the characteristics of black holes is having an unstable photon sphere. Additionally, the broader spatial coverage of the topological photon sphere study method around the gravitational structure is a key point that distinguishes it from the metric function, meaning that it can be used to determine the gravitational influence range (in the form of black holes + naked singularities) on photon motion.

- One of the main objectives of this article is to classify the parameter space of the studied models based on the existence and topological position of photon and anti-photon spheres. This means that we can precisely determine which parameter range of the model corresponds to a black hole structure or naked singularity. For instance, we observe that when the structure is in the form of a naked singularity, one (or more) stable photon spheres always appear alongside an unstable photon sphere in the studied spacetime. In the effective potential representation, this manifests as the appearance of a minimum alongside a maximum. Therefore, based on the results of this study and similar studies [35, 89, 90], we can conclude that if a stable photon sphere is observed within the studied parameter range, this may indicate the possibility of the model existing in the form of a singularity. Note that for all

the concepts discussed thus far, the obtained ranges may not necessarily and entirely hold physical meaning. These ranges will be most meaningful when interpreted alongside other pre-existing physical conditions and constraints. Overall, this method can provide a comprehensive view of the behavior of ultra-gravitational structures and serve as an auxiliary equation, offering better insight into the impact of the effective components in the black hole dynamics of the model.

- Another achievement of this method is that we can adjust the system parameters to force the studied model to exhibit the desired behavior or, conversely, estimate the approximate parameter ranges of the model based on the presence of the photon sphere in a specific region of space. For example, in some gravitational studies, we require a gravitational structure that adheres to specific principles and behaviors. In such cases, when we require the model parameters to fall within a specific range while simultaneously maintaining the structure as a defined black hole, this method can play a significant role. To further clarify, in the Swampland conjecture model study, hypotheses such as the WGC require that the studied structure, while being overly charged, still maintains its black hole structure. In this work, we propose that for such scenarios, the topological behavior of the photon sphere can be used, and after the parameters are adjusted as desired, the topological photon sphere can be examined to determine whether optimal conditions can be achieved [89–92].

- Finally, during the formulation of a theory, parameters considered necessary by the theoretical framework are added. These parameters may conceptually have a defined range from the outset or lack any limitations. In this paper, we have attempted to address the question of what impact these theories, when incorporated into the black hole model action, will have on the behavior of the photon sphere for their permissible values. Additionally, from the perspective of the photon sphere, whether these parameters, with all previous permissible values, will lead to the natural behavior of the studied model or if new constraints must be applied to these parameters.

ACKNOWLEDGEMENTS

J. Sadeghi and M. A. S. Afshar thank the University of Mazandaran.

References

- [1] R. Goswami, P. S. Joshi, and P. Singh, *Phys. Rev. Lett.* **96**(3), 031302 (2006)
- [2] D. Christodoulou, *Annals of Mathematics* **149**(1), 183 (1999)
- [3] P. S. Joshi and I. H. Dwivedi, *Phys. Rev. D* **47**(12), 5357 (1993)
- [4] D. Pugliese and H. Quevedo, *Naked singularities and black hole Killing horizons*, In *New Frontiers in Gravitational*

- Collapse and Spacetime Singularities, (Singapore: Springer Nature Singapore), 2024 May 3 (pp. 337-373)
- [5] R. Goswami and P. S. Joshi, *Phys. Rev. D - Particles, Fields, Gravitation, and Cosmology*, **76**, 084026 (2007)
- [6] A. Ghosh, *Study of Orbital Dynamics in Singular and Regular Naked Singularity Space-times*, (2024), arXiv: 2401.10771
- [7] M. Wang, G. Guo, P. Yan *et al.*, *Chin. Phys. C* **48**, 105103 (2024), arXiv: 2307.16748
- [8] P. S. Joshi and S. Bhattacharyya, *Primordial naked singularities*, (2024), arXiv: 2401.14431
- [9] Y. Chen, P. Wang, and H. Yang, *Observations of Orbiting Hot Spots around Naked Singularities*, (2023), arXiv: 2309.04157
- [10] K. S. Virbhadra, *Phys. Rev. D* **60**(10), 104041 (1999); V. Deliyiski, G. Gyulchev, P. Nedkova *et al.*, *Observing naked singularities by the present and next-generation Event Horizon Telescope*, (2024), arXiv: 2401.14092
- [11] D. P. Viththani, A. B. Joshi, T. Bhanja *et al.*, *Eur. Phys. J. C* **84**, 383 (2024)
- [12] K. Mosani, D. Dey, and P. S. Joshi, *Phys. Rev. D* **101**, 044052 (2020)
- [13] K. Acharya, K. Pandey, P. Bambhaniya *et al.*, *Naked singularity as a possible source of ultra-high energy cosmic rays*, (2023), arXiv: 2303.16590
- [14] R. Goswami and P. S. Joshi, *Class. and Quantum Grav.* **21**(15), 3645 (2004)
- [15] A. Kazunori *et al.*, *The Astrophysical Journal Letters* **875**, L5 (2019)
- [16] B. P. Abbott *et al.*, *Phys. Rev. X* **9**, 031040 (2019)
- [17] B. P. Abbott, R. Abbott, T. Abbott *et al.*, *Phys. Rev. Lett.* **116**, 061102 (2016)
- [18] K. Akiyama *et al.*, *The Astrophysical Journal Letters* **875**, 041301 (2019)
- [19] Event Horizon Telescope Collaboration, *First M87 event horizon telescope results. IV. Imaging the central supermassive black hole*, (2019), arXiv: 1906.11241
- [20] Event Horizon Telescope Collaboration, *First Sagittarius A* Event Horizon Telescope Results. VI: Testing the Black Hole Metric*, (2023), arXiv: 2311.09484
- [21] P. V. P. Cunha, C. A. R. Herdeiro, and E. Radu, *Phys. Rev. D* **96**, 024039 (2017)
- [22] C. R. Raúl and E. Astrid, *Black hole horizons must be veiled by photon spheres*, (2024), arXiv: 2405.08872
- [23] V. Cardoso *et al.*, *Phys. Rev. D* **90**, 044069 (2014); V. Cardoso, A. S. Miranda, E. Berti *et al.*, *Phys. Rev. D — Particles, Fields, Gravitation, and Cosmology* **79**(6), 064016 (2009)
- [24] P. V. P. Cunha and A. R. Carlos Herdeiro, *Phys. Rev. Letters* **124**, 181101 (2020)
- [25] S. W. Wei, *Phys. Rev. D* **102**, 064039 (2020)
- [26] J. Sadeghi, M. A. Afshar, S. N. Gashti *et al.*, *Astroparticle Physics* **156**, 102920 (2024)
- [27] P. V. P. Cunha, B. Emanuele, and A. R. Herdeiro Carlos, *Phys. Rev. Lett.* **119**, 251102 (2017)
- [28] *A Poincaré section is a lower-dimensional subspace of the state space of a continuous dynamical system that intersects a periodic orbit transversally and maps the points of intersection as a discrete dynamical system.*
- [29] Y. S. Duan, *The structure of the topological current*, SLAC-PUB-3301, (1984)
- [30] K. Akiyama, A. Alberdi, W. Alef *et al.*, *ApJL* **875**(1), L2 (2019); Event Horizon Telescope Collaboration, *ApJL*, **875**(1), L1 (2019); K. Akiyama, A. Alberdi, W. Alef *et al.*, *ApJL* **930**(2), L12 (2022)
- [31] S. Iftikhar, *Eur. Phys. J. C* **83**(2), 183 (2023); G. P. Li, H. B. Zheng, K. J. He *et al.*, *The shadow and observational images of the non-singular rotating black holes in loop quantum gravity*, (2024), arXiv: 2410.17295
- [32] A. K. Mishra, S. Chakraborty, and S. Sarkar, *Phys. Rev. D* **99**(10), 104080 (2019); G. S. Bisnovatyi-Kogan, O. Y. Tsupko, and V. Perlick, *Shadow of black holes at local and cosmological distances*, (2019), arXiv: 1910.10514
- [33] M. Fathi, M. Olivares, and J. R. Villanueva, *The European Physical Journal Plus*. **138**(1), 1-26 (2023); E. Teo, *General Relativity and Gravitation* **35**, 1909-26 (2003)
- [34] P. Morgan, *Annals of Physics* **414**, 168090 (2020)
- [35] J. Sadeghi and M. A. Afshar, *Astroparticle Physics* **162**, 102994 (2024)
- [36] Y. Sekhmani, S. N. Gashti, M. A. Afshar *et al.*, *Thermodynamic topology of Black Holes in $S F(R)$ S -Euler-Heisenberg gravity's Rainbow*, (2024), arXiv: 2409.04997
- [37] S. N. Gashti, M. A. Afshar, M. R. Alipour *et al.*, *Thermodynamic Topology of Kiselev-AdS Black Holes within $f(R, T)$ gravity*, (2024), arXiv: 2410.02262
- [38] S. W. Wei, Y. X. Liu, and R. B. Mann, *Phys. Rev. Lett.* **129**(19), 191101 (2022)
- [39] S. W. Wei, Y. X. Liu, and R. B. Mann, *Phys. Rev. D* **110**(8), L081501 (2024)
- [40] D. Wu and S. Q. Wu, *Phys. Rev. D* **107**(8), 084002 (2023)
- [41] D. Wu, S. Y. Gu, X. D. Zhu *et al.*, *JHEP* **2024**(6), 213 (2024)
- [42] X. D. Zhu, W. Liu, and D. Wu, *Phys. Lett. B* **29**, 139163 (2024)
- [43] X. D. Zhu, D. Wu, and D. Wen, *Phys. Lett. B* **856**, 138919 (2024), arXiv: 2402.15531
- [44] W. Liu, L. Zhang, D. Wu *et al.*, *Thermodynamic topological classes of the rotating, accelerating black holes*, (2024), arXiv: 2409.11666
- [45] D. Wu, W. Liu, S. Q. Wu *et al.*, *Novel Topological Classes in Black Hole Thermodynamics*, (2024), arXiv: 2411.10102
- [46] H. Chen, D. Wu, M. Y. Zhang *et al.*, *Physics of the Dark Universe* **46**, 101617 (2024)
- [47] J. Sadeghi, S. N. Gashti, M. R. Alipour *et al.*, *Annals of Physics* **455**, 169391 (2023)
- [48] M. R. Alipour, M. A. Afshar, S. N. Gashti *et al.*, *Physics of the Dark Universe* **42**, 101361 (2023)
- [49] J. Sadeghi, M. A. Afshar, S. N. Gashti *et al.*, *Annals of Physics* **460**, 169569 (2024)
- [50] J. Sadeghi, M. R. Alipour, S. N. Gashti *et al.*, *Bulk-boundary and RPS Thermodynamics from Topology perspective*, (2023), arXiv: 2306.16117
- [51] J. Sadeghi, M. A. Afshar, S. N. Gashti *et al.*, *Physica Scripta* **99**(2), 025003 (2024)
- [52] D. Wu, *Eur. Phys. J. C* **83**(5), 365 (2023)
- [53] D. Wu, *Eur. Phys. J. C* **83**(7), 589 (2023)
- [54] D. Wu, *Phys. Rev. D* **108**, 084041 (2023)
- [55] D. Wu, *Phys. Rev. D* **107**, 024024 (2023)
- [56] A. I. Lonappan *et al.*, *Phys. Rev. D* **97**, 043524 (2018)
- [57] A. R. Ade, Peter *et al.*, *Astronomy, Astrophysics* **571**, A1 (2014)
- [58] Carroll, Sean M. Dark Matter, *Dark Energy: The Dark Side of the Universe. Parts 1, 2. Teaching Company*, (2007)
- [59] V. C. Rubin, W. K. Jr Ford, and N. Thonnard, *Astrophysical Journal* **238**, 471 (1980)
- [60] M. Persic, S. Paolo, and S. Fulvio, *Monthly Notices of the*

- Royal Astronomical Society **281**(1), 27 (1996)
- [61] K. Akiyama, A. Alberdi, W. Alef *et al.*, *The Astrophysical Journal Letters* **930**(2), L15 (2022)
- [62] K. Akiyama, A. Alberdi, W. Alef *et al.*, *The Astrophysical Journal Letters* **930**(2), L14 (2022)
- [63] G. Bertone and H. Dan, *Reviews of Modern Physics* **90**, 045002 (2018)
- [64] X. Liang *et al.*, *Eur. Phys. J. C* **83**(11), 1009 (2023)
- [65] G. Abbas and R. H. Ali, *Eur. Phys. J. C* **83**(5), 1 (2023)
- [66] A. Das, S. Ashis, and G. Sunandan, *Class. and Quantum Grav.* **38**, 065015 (2021)
- [67] Q. Yu, X. Qi, and T. Jun, *Commun. Theor. Phys.* **75**, 095402 (2023)
- [68] R. Ruffini, Y. B. Wu, and S. S. Xue, *Phys. Rev. D* **88**, 085004 (2013)
- [69] D. Magos and B. Nora, *Phys. Rev. D* **102**, 084011 (2020)
- [70] Y. Xu *et al.*, *Chin. Phys. C* **46**, 115102 (2022)
- [71] S. J. Ma *et al.*, *Eur. Phys. J. C* **84**, 595 (2024), arXiv: 2401.03187
- [72] J. Bardeen, *Non-singular general relativistic gravitational collapse*, Proceedings of the 5th International Conference on Gravitation and the Theory of Relativity, (1968)
- [73] A. B. Eloy and G. Alberto, *Phys. Rev. Lett.* **80**(23), 5056 (1998)
- [74] A. B. Eloy and G. Alberto, *Phys. Lett. B* **493**(1-2), 149 (2000)
- [75] C. J. Gao, *Phys. Rev. D* **104**, 064038 (2021)
- [76] C. M. Claudel, S. V. Kumar, and F. R. E. George, *Journal of Mathematical Physics* **42**(2), 818 (2001)
- [77] S. Guo *et al.*, *Class. and Quantum Grav.* **38**, 165013 (2021)
- [78] S. W. Wei *et al.*, *Phys. Rev. Res.* **5**, 043050 (2023)
- [79] Y. Heydarzade and V. Vitalii, *Eur. Phys. J. C* **84**, 582 (2024)
- [80] E. Franzin, L. Stefano, and V. Vania, *Journal of Cosmology and Astroparticle Physics* **01**, 020 (2024)
- [81] Y. Koga *et al.*, *Phys. Rev. D* **105**, 104040 (2022)
- [82] P. Grandclément, *Phys. Rev. D* **95**, 084011 (2017)
- [83] S. Hod, *Phys. Lett. B* **776**, 1 (2018)
- [84] da Silva, Luís F. Dias *et al.*, *Phys. Rev. D* **108**, 084055 (2023)
- [85] Y. Koga and H. Tomohiro, *Phys. Rev. D* **100**, 064040 (2019)
- [86] P. V. P. Cunha, A. R. H. Carlos, and P. A. N. João, *Phys. Rev. D* **109**, 064050 (2024)
- [87] K. Mosani, D. Dipanjan, and S. J. Pankaj, *Monthly Notices of the Royal Astronomical Society* **504**(4), 4743 (2021)
- [88] K. S. Virbhadra and F. R. E. George, *Phys. Rev. D* **62**, 084003 (2000); K. S. Virbhadra, *Phys. Rev. D* **79**, 083004 (2009)
- [89] M. A. Afshar, J. Sadeghi, *Mutual Influence of Photon Sphere and Non-Commutative Parameter in Various Non-Commutative Black Holes: Part I-Towards evidence for WGC*, (2024), arXiv: 2411.09557
- [90] M. R. Alipour, M. A. Afshar, S. N. Gashti *et al.*, *Weak Gravity Conjecture Validation with Photon Spheres of Quantum Corrected AdS-Reissner-Nordstrom Black Holes in Kiselev Spacetime*, (2024), arXiv: 2410.14352
- [91] M. A. Afshar and J. Sadeghi, *Mutual Influence of Photon Sphere and Non-Commutative Parameter in Various Non-Commutative Black Holes: Part I-Towards evidence for WGC*, (2024), arXiv: 2411.09557
- [92] M. A. Afshar and J. Sadeghi, *Mechanisms Behind the Aschenbach Effect in Non-Rotating Black Hole Spacetime*, (2024), arXiv: 2412.06357